ELSEVIER

Coordination Chemistry Reviews
177 (1998) 181–199

COORDINATION CHEMISTRY REVIEWS

A quantum chemical investigation of the metal-to-ligand charge-transfer photochemistry

D. Guillaumont, C. Daniel *

Laboratoire de Chimie Quantique, UPR 139 du CNRS, Université Louis Pasteur, 4 Rue Blaise Pascal, 67000 Strasbourg, France

Received 17 November 1997; accepted 20 April 1998

Contents

Abstract

According to a number of recent experiments reported for a class of α-diimine mono- and di-nuclear transition metal carbonyls, these molecules may either photodissociate leading to highly reactive intermediates or manifest the photophysics of metal-to-ligand-charge-transfer

* Corresponding author. Tel.: +33 3 88416076; fax: +33 3 88416076; e-mail: daniel@quantix.u-strasbg.fr

PII S0010-8545(98)00133-7

(MLCT) complexes. The duality between these two extremes of behavior may be used to promote different applications like catalytic activity or energy/electrons transfers. The potential energy surfaces (PESs) associated with the low-lying singlet and triplet excited states of $Mn(H)(CO)_3(DAB)$ (DAB = 1,4-diaza-1,3-butadiene) calculated for the Mn–H bond homolysis and for the dissociation of an axial carbonyl ligand illustrate the complexity and the richness of the photochemistry and photophysics of this class of molecules. It is shown that the presence of significant energy barriers on the reaction path corresponding to the homolysis of the Mn–H bond are responsible for the low efficiency of this process in related complexes. The simulation of the dynamics of the ^{1}MLCT excited state, calculated at 26000 cm^{-1} and contributing mainly to the visible absorption spectrum, indicates that the most probable primary reaction is an ultrafast dissociation (< 200 fs) of the carbonyl ligand. The relative positions of the quasi-bound MLCT states with respect to the sigma bond-to-ligand-charge-transfer (SBLCT) excited state corresponding to the $\sigma_{Mn-H} \rightarrow \pi^*_{DAB}$ excitation will govern the photoreactivity of the molecules. A comparative study of the sequence, the nature of the low-lying excited states and of the associated state correlation diagrams for the hydride complex and the ethyl analog $Mn(Et)(CO)_3(DAB)$ points to a better reactivity of the ethyl-substituted complex in agreement with the experimental data. This is a consequence of a lowering of the excited states, an increase in the density of states in the visible energy domain and a mixing of the triplet SBLCT and MLCT states on going from the hydride to the ethyl complex. The influence of the metal center on going from the manganese to the rhenium compound is expressed by an important mixing of the MLCT and SBLCT states and a lowering of the excited states due to a relativistic destabilization of the d shells of the metal center and an indirect stabilization of the π^*_{DAB} orbital through its interaction with the 6p of the rhenium. These heavy atom effects should induce a better photoreactivity for the third-row transition metal complexes than for the first-row analogs.

Keywords: Photochemistry; Quantum chemical calculations; Metal-to-ligand-charge-transfer

1. Introduction

According to a number of experiments [1–6] reported for a class of α-diimine mono- and di-nuclear transition metal carbonyls these molecules may either photodissociate, leading to unsaturated intermediates, or display the photophysics of metal-to-ligand-charge-transfer (MLCT) excited states. This dual behavior may be used to advance different applications, such as catalytic activity or energy/electrons transfer. Recent examples, reported for $M(R)(CO)_3$(α-diimine) complexes (M = Mn, Re; R = methyl, ethyl, benzyl) [7–10], indicate that the Re–R bond homolysis is the major primary reaction for R = ethyl, benzyl, whereas the Re–methyl bond homolysis is a minor photodissociation process, 60% of irradiated $Re(Me)(CO)_3$(bipyridine) leading to an efficient emission attributed to the low-lying ^{3}MLCT excited states. For the first time a branching ratio between direct homolysis of an alkyl–metal bond and deactivation through emission has been measured indicating that only 40% of $Re(Me)(CO)_3$(bipyridine) dissociates toward the homolysis primary products. When the rhenium center is replaced by a manganese atom,

the only observed photodissociation channel is the loss of a carbonyl for R = methyl, whereas the benzyl-substituted analog is characterized by the homolysis of the Mn–R bond with a quantum yield of 0.4. Several other examples illustrate the complexity and the richness of this family of molecules with a variety of substituents, metal centers and α-diimine ligands [11–14]. A tentative rationalization of this fascinating photochemical behavior, based on detailed investigations of the spectral properties (time-resolved absorption/emission spectra, resonance Raman, UV-photoelectron spectroscopy), supplemented by a qualitative analysis in terms of bonding/antibonding molecular orbitals has been proposed for a number of molecules [15–18]. However, despite this intense activity, little is known regarding the ordering of the low-lying excited states, their nature or their dissociative character. The mechanism of photodissociation seems to be governed by the nature of the so-called sigma-bond-to-ligand-charge-transfer (SBLCT) excited state which can either present the characteristics of the long life time MLCT state or dissociate towards radical formation in a sub-nanosecond time scale. The experimental conditions, the metal center, the α-diimine ligands and the substituent R are many factors which will largely influence the response of this class of molecules to visible light.

In order to investigate the electronic spectrum of these molecules we have studied the nature of the low-lying excited states in a series of $M(R)(CO)_3(DAB)$ (M = Mn, R = H, methyl, ethyl; M = Re, R = H; DAB = 1-4-diaza-1,3-butadiene) complexes and calculated the relative excitation energies at the CASSCF (complete active space SCF) MR/CCI (multireference contracted CI) level [19]. A mechanism of photodissociation, based on the calculation of the potential energy surfaces (PESs) as a function of the Mn–H and the $Mn–CO_{ax}$ bonds elongation in $Mn(H)(CO)_3(DAB)$ has been proposed [20,21]. The key to this mechanism is the occurrence of energy barriers along the homolysis reaction path generated by avoided crossings between the ^{3}SBLCT dissociative state, corresponding to an excitation from the metal–hydrogen $\sigma_{Mn\ H}$ bonding orbital to the π^*_{DAB} vacant orbital of the DAB ligand, and the low-lying ^{3}MLCT excited states of the same symmetry. More recently, simulation of the ultra-fast dynamics (in a femtosecond time scale) of the $Mn(H)(CO)_3(DAB)$ excited states has been undertaken.

The aim of the present contribution is to bring to the attention of experimental spectroscopists and photochemists the latest theoretical developments in this field. The first part of this work describes the simulation of the photodissociation dynamics of the simple $Mn(H)(CO)_3(DAB)$ molecule, based on wavepacket propagation on two-dimensional (2D) PESs calculated as a function of the reaction coordinates $q_a = Mn–H$ and $q_b = Mn–CO_{ax}$. The second part of this paper is dedicated to a qualitative investigation of the influence of the metal center and of the nature of the substituents on the observed photochemistry. This qualitative analysis is based on the knowledge of the relative position and of the nature of the low-lying excited states in several $M(R)(CO)_3(DAB)$ complexes completed by an interpretation in terms of state correlation diagrams.

2. Computational methods

2.1. Quantum chemical calculations

The calculations have been carried out under the C_s symmetry constraint for idealized geometries of the $M(R)(CO)_3(DAB)$ complexes (Fig. 1) with the bond lengths and bond angles given in Ref. [22]. The following Gaussian basis sets were used for the manganese compounds, for which all-electron calculations were performed: for the manganese atom either a (15, 11, 6) set contracted to [9, 6, 3] (for $Mn(H)(CO)_3(DAB)$)[1] or a (14, 9, 6) set contracted to [6, 4, 3] (for R = methyl, ethyl)[2]; for the first row atoms either a (10, 6) set contracted to [4, 2] (for $MnH(CO)_3(DAB)$) [25] or a (9, 5) set contracted to [3, 2] (for R = methyl, ethyl) [25]; for hydrogen atoms either a (6, 1) set contracted to [3, 1] (for the atom directly linked to the metal center) [26] or a (4) set contracted to [2] for the other hydrogen atoms [26]. The following Gaussian basis sets were used for the rhenium complex studied in the relativistic effective core potential (ECP) (small core) approximation: for the rhenium atom ($Z = 15.0$) a (8, 7, 6) set contracted to [6, 5, 3] [27]; for the carbon ($Z = 4.0$) and nitrogen ($Z = 5.0$) atoms a (4, 4) set contracted to [2, 2] [28]; for the oxygen ($Z = 6.0$) atoms a (4, 5) set contracted to [2, 3] [28]. The same basis sets were used for the hydrogen atoms in the manganese and rhenium complexes.

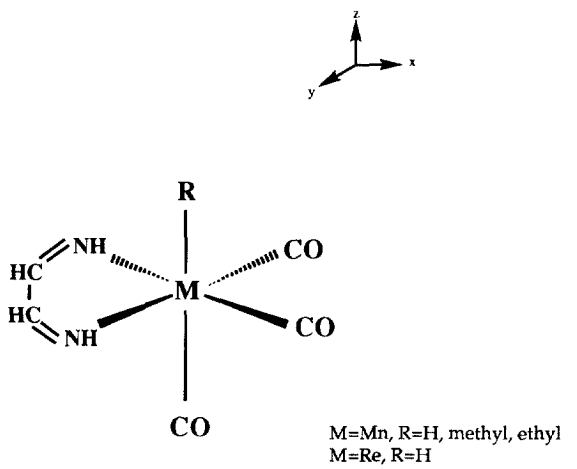

Fig. 1. Idealized geometry of $M(R)(CO)_3(DAB)$ (M = Mn, R = H, Me, Et; M = Re, R = H).

[1] This basis set is made from the (14, 9, 5) basis of Wachters [23] by adding an additional *s* function (exponent 0.3218), two diffuse *p* functions and one diffuse *d* function.

[2] This basis set is made from the (13, 7, 5) basis set of Ref. [24] by adding an additional *s* function (exponent 0.2732) and two *p* functions (exponents 0.2021 and 0.06516) and replacing the last *d* function with two *d* functions (exponents 0.2584 and 0.08231).

The ab initio calculations were performed at the correlated level (CASSCF, CCI) [29,30] in order to describe properly the correlation effects which cannot be neglected in transition metal complexes[3]. The choice of the correlated electrons and the determination of the CASSCF active space, as well as the size of the CI calculation and the number of reference configurations, is governed by our concern for a balanced description of the different electronic states (ground and excited) in the Franck–Condon (FC) region and at dissociation [20,21,34–36].

2.1.1. Excited states

Calculations have been performed for the a^1A' electronic ground states corresponding to the $(\sigma_{M-R})^2(3d_{x^2-y^2})^2(3d_{yz})^2(3d_{xz})^2$ electronic configuration and for the low-lying $^{1,3}A'$ excited state corresponding to the $(\sigma_{M-R})^2(3d_{x^2-y^2})^2(3d_{yz})^2(3d_{xz})^1(\pi^*_{DAB})^1$, $(\sigma_{M-R})^2(3d_{x^2-y^2})^1(3d_{yz})^2(3d_{xz})^2(\pi^*_{DAB})^1$ and $(\sigma_{M-R})^1(3d_{x^2-y^2})^2(3d_{yz})^2(3d_{xz})^2(\pi^*_{DAB})^1$ electronic configurations with the conformation depicted in Fig. 1. CASSCF calculations, averaged over the low-lying states of a given symmetry and spin, were performed in order to generate a set of molecular orbitals used in a subsequent multireference CI. Our interest centered mostly on the lowest excited states corresponding to $d \rightarrow d$, $d \rightarrow \pi^*_{DAB}$ and $\sigma_{M-R} \rightarrow \pi^*_{DAB}$ excitations. Eight electrons were correlated (the 3d electrons and the two electrons involved in the M–R bond) in either ten (R = H, methyl) or nine (R = ethyl) orbitals corresponding to the 3d and 4d orbitals which correlate them, the σ_{M-R} and σ^*_{M-R} orbitals (σ_{M-R} and σ^*_{M-R} orbitals denote the molecular orbitals that are bonding and antibonding with respect to the M–R bond respectively) and the lowest π^*_{DAB} orbital localized on the DAB group. For each electronic state monoreference CCI calculation was followed by a multireference calculation, including all configurations with a coefficient larger than 0.08 in the monoreference CI. Single and double excitations to all virtual orbitals, except the counterparts of the carbonyls and diimine 1s and the metal 1s, 2s and 2p orbitals, are included. The same strategy was used for the computation of the PESs.

2.1.2. Potential energy surfaces

A systematic geometry optimization, including all degrees of freedom, at a correlated level for the different electronic states cannot be performed for such large transition metal complexes. On the basis of the experimental Stokes shifts, which are usually very small for this class of molecule [37], and of a limited evaluation of the geometrical relaxation effects on going from the electronic ground state to the low-lying excited states [38], the present study was restricted to the calculation of 2D PESs. The reaction coordinates are chosen on the basis of the experimental data (observed primary reactions, structures of the primary products) and of the main geometrical deformations between the electronic ground state and the low-lying excited states and on going from the FC region to the formation of the primary products. An illustration of the geometrical deformations on going from the

[3] The original program was interfaced for use in conjunction with the ASTERIX system of programs [31–33] by C. Daniel, M. Spéri, M. M. Rohmer.

electronic ground state (values in parentheses in Fig. 2) either to the ^{3}MLCT excited state (top of Fig. 2) or to the ^{3}SBLCT excited state (bottom of Fig. 2) is given in Fig. 2 for $Mn(H)(CO)_3(DAB)$. The main deformations in the ^{3}MLCT are an elongation of the axial carbonyl ligand and a shortening of the Mn–H bond. The metal equatorial carbonyls bond distances are less significantly modified. In contrast, the geometry optimization indicates an elongation of the Mn–H bond in the ^{3}SBLCT state and a shortening of the $Mn–CO_{ax}$ bond. The angular

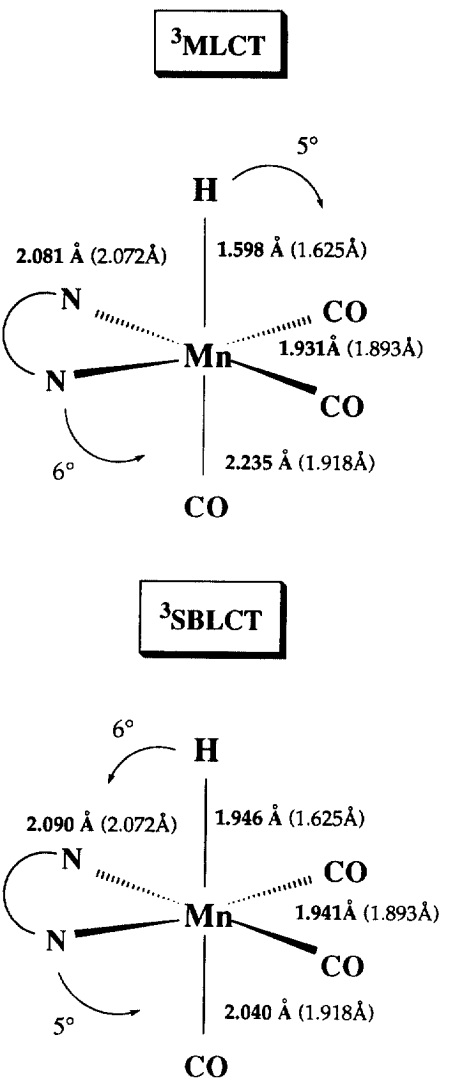

Fig. 2. Gradient/CASSCF optimized geometries of the lowest ^{3}MLCT and ^{3}SBLCT excited states in $Mn(H)(CO)_3(DAB)$ (the electronic ground state bond distances are given in parentheses).

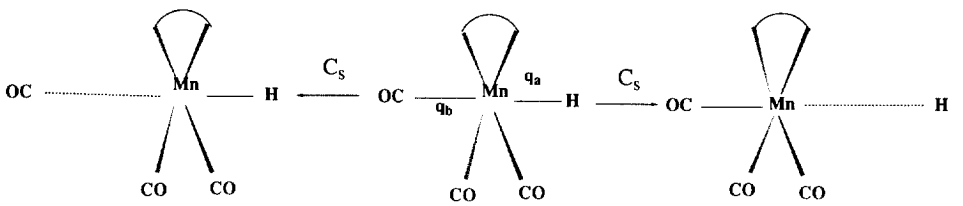

Scheme 1.

deformations are evaluated to be $< 10°$ on going from the ground state to both excited states.

In the present work, the highest possible symmetry is retained along the reaction pathways. Consequently, the dissociation of an equatorial carbonyl is not considered in the simulation. The photodissociation of $Mn(H)(CO)_3(DAB)$ has been studied under the C_s symmetry constraint (Scheme 1) and modeled as a pseudotriatomic system with two collinear dissociative bonds, $q_a = [Mn–H]$ and $q_b = [Mn–CO_{ax}]$.

The potentials for the electronic ground states and the lowest excited states of $Mn(H)(CO)_3(DAB)$ molecules are modeled by fitting analytical functions to CASSCF/MR-CCI ab initio points, with additional smoothing to avoid any obvious artefact such as shallow minima in the asymptotic domain.

2.2. Excited states dynamics

The photoabsorption and the dynamics of the excited states are simulated by propagation of selected wavepackets $\Psi_e(q_a, q_b, t)$ on the potentials corresponding to the e excited states. The time evolution of the wavepackets is obtained by solving the time-dependent Schrödinger equation:

$$i\hbar \frac{\partial}{\partial t} \Psi_e(q_a, q_b, t) = [T_{nu} + V_e]\Psi_e(q_a, q_b, t) \tag{1}$$

with the initial conditions

$$\Psi_e(q_a, q_b, t = 0) = \mu_e \Phi_{gs,0}(q_a, q_b) \tag{2}$$

where μ_e is the electronic transition moment between the ground state (gs) and the excited state e. $\Phi_{gs,0}(q_a, q_b)$ represents the 2D vibrational ground wavefunction of the electronic ground state evaluated through the Fourier grid Hamiltonian method [39,40]. The solution of the time-dependent Schrödinger Eq. (1) is obtained by the second-order-differential propagation scheme with $\Delta t = 7.0 \times 10^{-3}$ fs [41].

The kinetic part of the Hamiltonian of the system, expressed in bond coordinates, is given by

$$T_{nu} = -\frac{\hbar^2}{2\mu_a}\frac{\partial^2}{\partial q_a^2} - \frac{\hbar^2}{2\mu_b}\frac{\partial^2}{\partial q_b^2} + \frac{\hbar^2}{m_c}\frac{\partial^2}{\partial q_a \partial q_b} \quad (3)$$

where m_c is the mass of the central atom and μ_a and μ_b are the reduced masses corresponding to the bonds q_a and q_b. The propagations are based on representations of $\Psi_e(q_a, q_b, t)$ on 2D grids corresponding to the reaction coordinates with the following parameters: $q_{a_i} = q_{a_0} + (i-1)\Delta q_a$, $q_{a_0} = 1.0$ a.u., $\Delta q_a = 0.1$ a.u. with $1 \leq i \leq 32$ and $q_{b_i} = q_{b_0} + (i-1)\Delta q_b$, $q_{b_0} = 1.4$ a.u., $\Delta q_b = 0.03$ a.u. with $1 \leq i \leq 256$.

3. Photodissociation dynamics of $Mn(H)(CO)_3(DAB)$

3.1. Potential energy surfaces

A set of adiabatic PESs for the electronic ground and excited states of $Mn(H)(CO)_3(DAB)$, selected from the 2D PESs calculated under the C_s symmetry constraint for the b^1A' and c^1A' singlet MLCT states, corresponding to the $3d_{x^2-y^2} \rightarrow \pi^*_{DAB}$ and $3d_{xz} \rightarrow \pi^*_{DAB}$ excitations respectively, and the d^1A' SBLCT state corresponding to the $\sigma_{Mn-H} \rightarrow \pi^*_{DAB}$ excitation are represented in Fig. 3. The low-lying MLCT states, calculated at $21385 \pm 325\ cm^{-1}$ and $26315 \pm 315\ cm^{-1}$ respectively [19,21], are quasi-bound for the Mn–H elongation, whereas they are weakly dissociative with respect to the axial carbonyl dissociation.

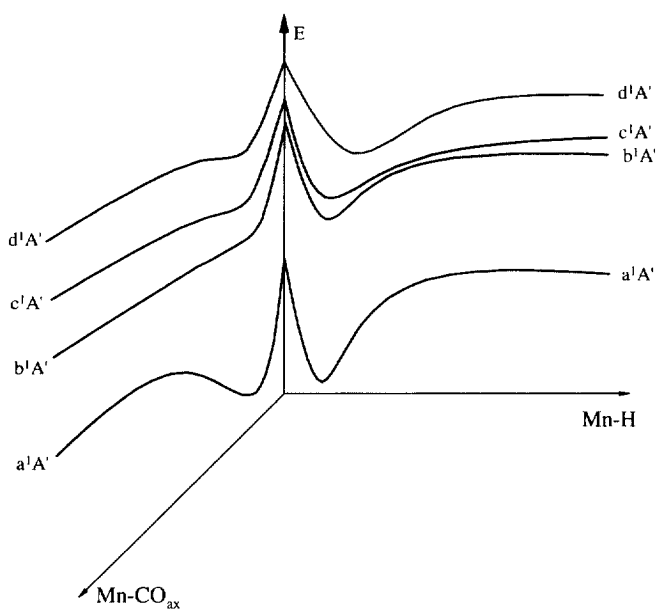

Fig. 3. Sets of CASSCF/MRCI potential energy curves calculated for the low-lying singlet states as a function of the Mn–H and Mn–CO_{ax} bonds elongations in $Mn(H)(CO)_3(DAB)$.

The ^{1}SBLCT excited state, calculated at 37950 cm^{-1} [19] or 37980 cm^{-1} [21], has a quasi-bound character in both directions (q_a = Mn–H and q_b = Mn–CO_{ax}). This state should not participate directly in the photodissociation of Mn(H)$(CO)_3$(DAB). A set of the corresponding adiabatic triplet PESs is represented in Fig. 4. Owing to the presence of avoided crossings between the dissociative ^{3}SBLCT state and the low-lying ^{3}MLCT states, significant energy barriers are generated along the Mn–H homolysis reactive channel, particularly on the lowest a^3A' adiabatic PES which shows a potential well around the equilibrium distance (q_a = 1.576 Å) and a dissociative character at long distances (q_a > 1.8 Å).

In contrast, the low-lying ^{3}MLCT (a^3A' and b^3A') states are nearly dissociative for the dissociation of an axial carbonyl ligand whereas the ^{3}SBLCT (c^3A') state is attractive in this direction. The shape of the PESs represented in Figs. 3 and 4 accounts for a qualitative understanding of the mechanism of photodissociation of Mn(H)$(CO)_3$(DAB):

1. under irradiation in the visible, the system gets trapped into the potential wells of the low-lying b^1A' and c^1A' MLCT states.
2. the system may dissociate towards the CO + Mn(H)$(CO)_2$(DAB) primary products, either directly from these ^{1}MLCT states in an ultra-fast direct scheme, or from the low-lying ^{3}MLCT states through an indirect mechanism via ^{1}MLCT → ^{3}MLCT intersystem crossing (ISC).

The homolysis of the Mn–H bond should account for a minor primary reaction with an extremely low quantum yield, owing to the presence of high energy barriers along the corresponding channel of dissociation.

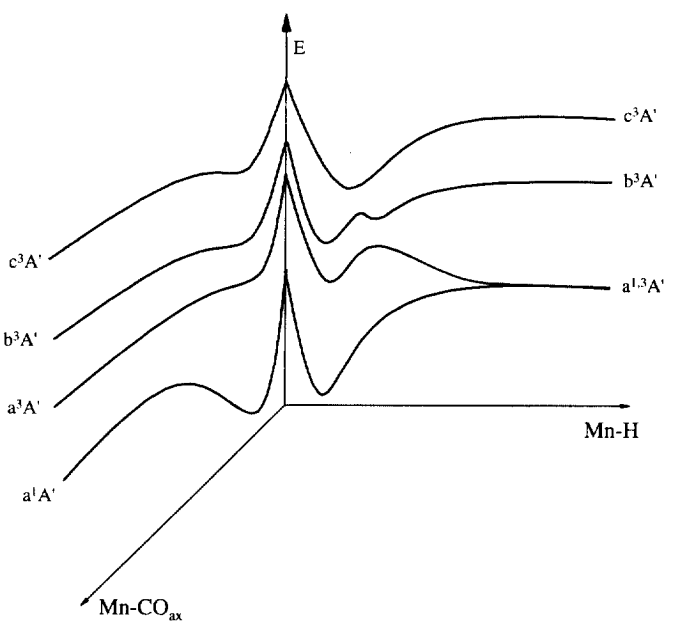

Fig. 4. Sets of CASSCF/MRCI potential energy curves calculated for the low-lying triplet states as a function of the Mn–H and Mn–CO_{ax} bonds elongations in Mn(H)$(CO)_3$(DAB).

3.2. Excited states

According to our recent calculations [19], the two low-lying ^{1}MLCT states range between 21000 and 26000 cm^{-1} and the calculated oscillator strengths indicate that the c^1A' state corresponding mainly to the $3d_{xz} \rightarrow \pi^*_{DAB}$ excitation is more likely to be populated under visible irradiation. The three low-lying singlet excited states are well characterized in the FC region and remain nearly pure along both dissociative channels (carbonyl loss and Mn–H homolysis).

The situation is much more complicated for the low-lying triplet states. In the FC domain and along the CO dissociation pathway, the ^{3}MLCT and ^{3}SBLCT excited states remain nearly pure. However, as soon as the system leaves the equilibrium geometry towards the primary products of the homolysis an important mixing between the ^{3}SBLCT and the two low-lying ^{3}MLCT states makes the analysis in terms of molecular orbitals doubtful at this stage of the mechanism. Indeed, around the avoided crossings region (between 1.8 and 2.5 Å) the mixed character of the wavefunctions illustrates an abrupt change of electronic configuration. In particular, the nature of the lowest adiabatic a^3A' PES is modified from pure bound MLCT (around 1.576 Å) to dissociative character (after 2.0 Å). At the same time, the nature of the acceptor orbital is modified, becoming a mixture of π^*_{DAB} and $3d_{z^2}$ metal localized orbital (Scheme 2). At dissociation ($q_a = 50.0$ Å) the unpaired electron is totally delocalized over the $3d_{z^2}$ and π^*_{DAB} orbitals of the $Mn(CO)_3(DAB)$ fragment.

3.3. Dynamics of $HMn(CO)_3(DAB)$

3.3.1. Visible photochemistry

In order to follow the photochemical behavior of $Mn(H)(CO)_3(DAB)$ under irradiation in the visible we have performed 2D wavepacket propagations including the $q_a = [Mn–H]$ and $q_b = [Mn–CO_{ax}]$ reaction coordinates. Preliminary 1D propagations (along $q_a = [Mn–H]$) performed on the whole set of spin–orbit and non-adiabatically coupled electronically excited potentials: the low-lying b^1A' and c^1A' (^{1}MLCT) states (in the visible absorption domain), the d^1A' (^{1}SBLCT) state and the triplet a^3A', b^3A' (^{3}MLCT) and c^3A' (^{3}SBLCT) excited states, indicate a

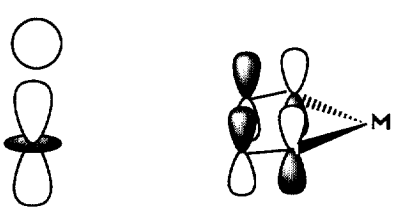

$\sigma_{M\text{-}R}$ π^*_{dab}

Scheme 2.

very inefficient singlet to triplet ISC process at the early stage of the simulation (below 500 fs) and a negligible contribution of the non-adiabatic coupling.

For these two reasons, the present 2D simulation has been achieved by propagation of the $\Psi_{c}^{1}A'(q_a, q_b, t)$ wavepacket on the corresponding non-coupled potential $V_{c}^{1}A'(q_a, q_b)$ (Fig. 5) by solving the time-dependent Schrödinger equations (Eq. (1)) with the following initial conditions:

$$\Psi_{c}^{1}A'(q_a, q_b, t=0) = \mu_{a}^{1}A' \rightarrow {}_{c}^{1}A'\Phi_{a}^{1}A'_{,0}(q_a, q_b) \tag{4}$$

and

$$\Psi_{b}^{1}A'(q_a, q_b, t=0) = \Psi_{d}^{1}A'(q_a, q_b, t=0) = 0 \tag{5}$$

$$\Psi_{a}^{3}A'(q_a, q_b, t=0) = \Psi_{b}^{3}A'b(q_a, q_b, t=0) = \Psi_{c}^{3}A'(q_a, q_b, t=0) \tag{6}$$

The corresponding snapshots of densities are shown in Fig. 6.

After the initial $a^1A' \rightarrow c^1A'$ transition, on a short time scale (< 75 fs) the wavepacket evolves to the dissociation channel corresponding to the axial CO elimination. The dissociation of the carbonyl ligand occurs on a time scale of the order of 200 fs. A fraction of the system remains trapped in the $V_{c}^{1}A'(q_a, q_b)$ potential well situated in the direction of the Mn–H bond elongation (Fig. 3). The system has insufficient energy to induce the breaking of the Mn–H bond. The only alternative of deactivation on a longer time scale will be either the CO loss or the unproductive decay to the electronic ground state from the low-lying triplet MLCT states.

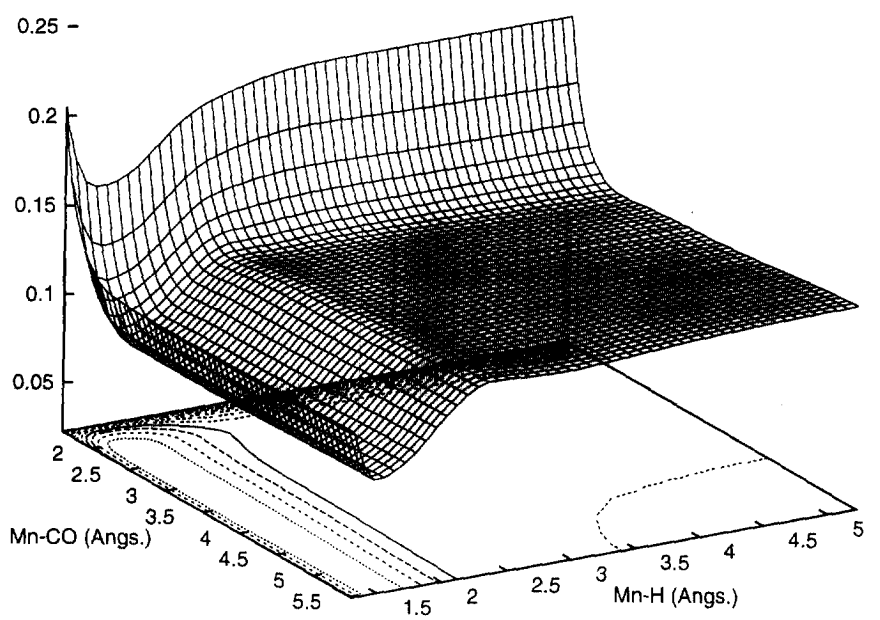

Fig. 5. Two-dimensional PES $V_{c}^{1}A'(q_a, q_b)$ associated with the c^1A' MLCT excited state used in the simulation of the 2D photodissociation dynamics.

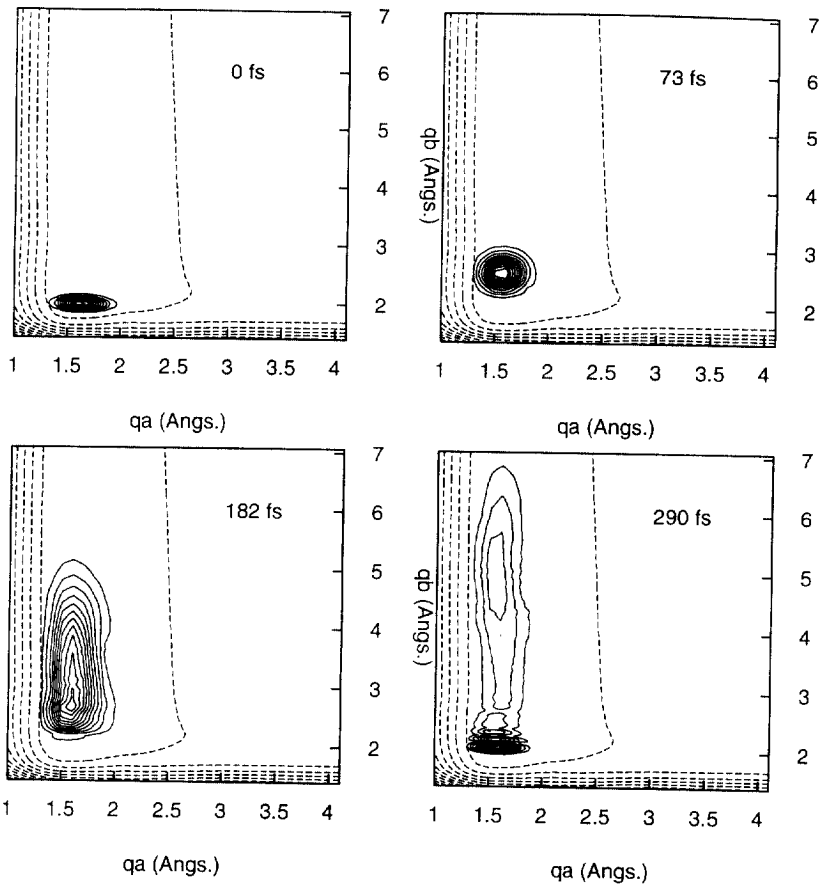

Fig. 6. Time evolution of the $\Psi_{1_{cA}}(q_a, q_b, t)$ (solid line) wavepacket on the $V_{1_{cA}}(q_a, q_b)$ (dashed line) potential as a function of $q_a = [Mn–H]$ and $q_b = [Mn–CO_{ax}]$.

4. Influence of the radical R on the photoreactivity

4.1. Excited states

The main trends on going from the hydride $Mn(H)(CO)_3(DAB)$ to the ethyl $Mn(Et)(CO)_3(DAB)$ complex are a lowering of the excited states and a dramatic change of the nature of the low-lying triplet states. This lowering, which is a consequence of the stabilization of the π^*_{DAB} orbital on the one hand and of the weakening of the $\sigma_{Mn\ R}$ bond on the other hand is less important for the MLCT states (< 1.0 eV) than for the SBLCT states ($\gg 1.0$ eV). According to the results reported in Table 1, the excited states (singlets and triplets) of $Mn(H)(CO)_3(DAB)$ are nearly pure and correspond to excitations to the lowest π^*_{DAB} orbital of the α-diimine ligand, either from the 3d shells of the metal center (MLCT states) or from the metal–hydrogen σ-bonding orbital (SBLCT states).

Table 1
Calculated CASSCF/CCI excitation energies (cm^{-1}) to the lowest $^{1,3}A'$ excited states of $RM(CO)_3(DAB)$ (M = Mn, R = H, ethyl; M = Re, R = H) and one-electron excitation in the principal configurations [19]

Transition	M = Mn, R = H	M = Mn, R = ethyl	M = Re, R = H
$a^1A' \rightarrow a^3A'$	$3d_{xz} \rightarrow \pi^*_{DAB}$ (0.90)	$\sigma_{Mn-R} \rightarrow \pi^*_{DAB}$ (0.66) $3d_{xz} \rightarrow \pi^*_{DAB}$ (0.61)	$5d_x + \sigma_{Re-H} \rightarrow \pi^*_{DAB}$ (0.71) $\sigma_{Re-H} - 5d_{xz} \rightarrow \pi^*_{DAB}$ (0.64)
	15 090	11 080	12 600
$a^1A' \rightarrow b^3A'$	$3d_{x^2-y^2} \rightarrow \pi^*_{DAB}$ (0.88)	$3d_{xz} \rightarrow \pi^*_{DAB}$ (0.69) $\sigma_{Mn-R} \rightarrow \pi^*_{DAB}$ (0.58)	$5d_{x^2-y^2} \rightarrow \pi^*_{DAB}$ (0.90)
	19 200	12 280	13 710
$a^1A' \rightarrow b^1A'$	$3d_{x^2-y^2} \rightarrow \pi^*_{DAB}$ (0.90)	$3d_{xy} \rightarrow \pi^*_{DAB}$ (0.63) $3d_{x^2-y^2} \rightarrow \pi^*_{DAB}$ (0.61)	$5d_{x^2-y^2} \rightarrow \pi^*_{DAB}$ (0.91)
	21 060 ($f = 0.03$)	15 580	15 250 ($f = 0.0003$)
$a^1A' \rightarrow c^1A'$	$3d_{xz} \rightarrow \pi^*_{DAB}$ (0.75)	$3d_{x^2-y^2} \rightarrow \pi^*_{DAB}$ (−0.64) $3d_{xz} \rightarrow \pi^*_{DAB}$ (−0.53)	$5d_{xz} + \sigma_{Re-H} \rightarrow \pi^*_{DAB}$ (0.68) $\sigma_{Re-H} - 5d_{xz} \rightarrow \pi^*_{DAB}$ (0.44)
	26 000 ($f = 0.39$)	17 560	21 721 ($f = 0.32$)
$a^1A' \rightarrow c^3A'$	$\sigma_{Mn-H} \rightarrow \pi^*_{DAB}$ (0.89)	$3d_{x^2-y^2} \rightarrow \pi^*_{DAB}$ (0.89)	$\sigma_{Re-H} - 5d_{xz} \rightarrow \pi^*_{DAB}$ (0.69) $5d_{xz} + \sigma_{Re-H} \rightarrow \pi^*_{DAB}$ (0.59)
	34 390	16 200	27 650
$a^1A' \rightarrow d^3A'$	$\sigma_{Mn-H} \rightarrow \pi^*_{DAB}$ (0.80)	$\sigma_{Mn-R} \rightarrow \pi^*_{DAB}$ (0.82)	$\sigma_{Re-H} - 5d_{xz} \rightarrow \pi^*_{DAB}$ (0.64) $5d_{xz} + \sigma_{Re-H} \rightarrow \pi^*_{DAB}$ (0.59)
	37 950 ($f = 0.11$)	26 240	31 340 ($f = 0.12$)

In contrast, the low-lying triplet states of $Mn(Et)(CO)_3(DAB)$ exhibit a mixed character illustrated by the hybridization of the $3d_{xz}$ and $3d_{z^2}$ orbitals of the metal which increases the overlap between the metal center and the sp orbital of the ethyl. This mixed ^{3}(SBLCT/MLCT) composition for two of the three low-lying triplet states in the ethyl complex may greatly influence photochemical behavior. Moreover, the energy domain covered by the triplets is considerably reduced on going from the hydride (15090–34390 cm^{-1}) to the ethyl complex (11080–16200 cm^{-1}). This increase in the density of states in the visible energy domain should significantly affect the photoreactivity of the molecule.

On going from the hydride to the ethyl complex, the ordering and the nature of the low-lying singlet excited states are similar and well defined. Therefore, the shape of the absorption spectrum should not be dramatically modified inside the molecular series. Indeed, the experiments report common spectral features for different molecules [37]: an intense band in the visible, corresponding to the absorption from the electronic ground state to one of the low-lying ^{1}MLCT states, and a weak shoulder at higher energies, corresponding to the absorption of the ^{1}SBLCT state (with a significant contribution of a metal-centered ^{1}MC state corresponding to the $3d_{yz} \rightarrow 3d_{xy}$ excitation), in agreement with the theoretical absorption spectrum proposed for $Mn(H)(CO)_3(DAB)$ [19]. Similar calculations performed for the methyl analog $Mn(Me)(CO)_3(DAB)$ point to an intermediate photochemical behavior of the methyl complex that is closer to the hydride than to the ethyl compound.

4.2. State correlation diagrams

The state correlation diagrams connecting the electronic ground state and the lowest triplet excited states of the reactants $Mn(R)(CO)_3(DAB)$ to those of the homolysis primary products $R + Mn(CO)_3(DAB)$ are reported in Fig. 7(a) (R = H) and Fig. 7(b) (R = ethyl). The energy levels corresponding to the singlet excited states are shown for the reactants in order to situate the triplet states with respect to the absorption energy domain.

The state correlation diagrams are based on CASSCF/MR-CCI energies of the corresponding electronic states. An extreme situation is illustrated in Fig. 7(a) for $Mn(H)(CO)_3(DAB)$, where the ^{3}SBLCT dissociative state is well separated from the low-lying bound ^{3}MLCT states, well above the ^{1}MLCT states. The presence of energy barriers due to avoided crossings between the ^{3}SBLCT and ^{3}MLCT states makes the homolysis reaction very improbable. The state correlation diagrams corresponding to the breaking of the Mn–ethyl bond in $Mn(Et)(CO)_3(DAB)$ are represented in Fig. 7(b). The presence of the two largely mixed ^{3}(SBLCT/MLCT) states in the low energy domain prevents the occurrence of energy barriers along this reaction coordinate. Consequently, the ethyl dissociation reaction should be a very efficient primary reaction. Without the knowledge of the corresponding PESs it is untimely to propose a mechanism of deactivation of the ethyl complexes.

5. Influence of the metal center on the photoreactivity

The CASSCF/MR-CCI excitation energies to the lowest excited states of $Re(H)(CO)_3(DAB)$ are reported in Table 1. These results show two important trends on going from the manganese to the rhenium complex: (i) a lowering of the excitation energies; (ii) a strong mixing between the ^{1,3}MLCT and ^{1,3}SBLCT excited states. The lowering of the excited states is a direct consequence of the relativistic destabilization of the 5d shells and of the stabilizing interaction between the vacant π^*_{DAB} orbital and the $6p_z$ of the metal center. The lowest MLCT state, corresponding to the $5d_{x^2-y^2} \rightarrow \pi^*_{DAB}$ excitation remains pure in the rhenium analog, whereas the MLCT state corresponding to the $5d_{xz} \rightarrow \pi^*_{DAB}$ excitation exhibits a large mixture with the SBLCT state. This mixed state, calculated at 21 721 cm^{-1} with an oscillator strength of 0.32 (to be compared with the low value close to 0.0 for the lowest ^{1}MLCT state) agrees with the intense absorption band, at around 20 000 cm^{-1}, observed for this class of rhenium complexes [7–10]. The mixed character of this initially populated ^{1}(MLCT/SBLCT) state is probably responsible for the surprising photochemical behavior of the rhenium complex under visible irradiation: a very efficient homolysis (supposing dissociative potentials) coupled with the detection of a long life time triplet (250 ns) '$\sigma\pi^*$' excited state (characteristic of a bound state). Indeed, owing to this important change in the nature of the electronic state, the associated potential energy surface should differ substantially from the surface calculated for $Mn(H)(CO)_3(DAB)$ shown in Figs. 3 and 4. A nearly dissociative shape may be expected with a low energy barrier at long Re–R

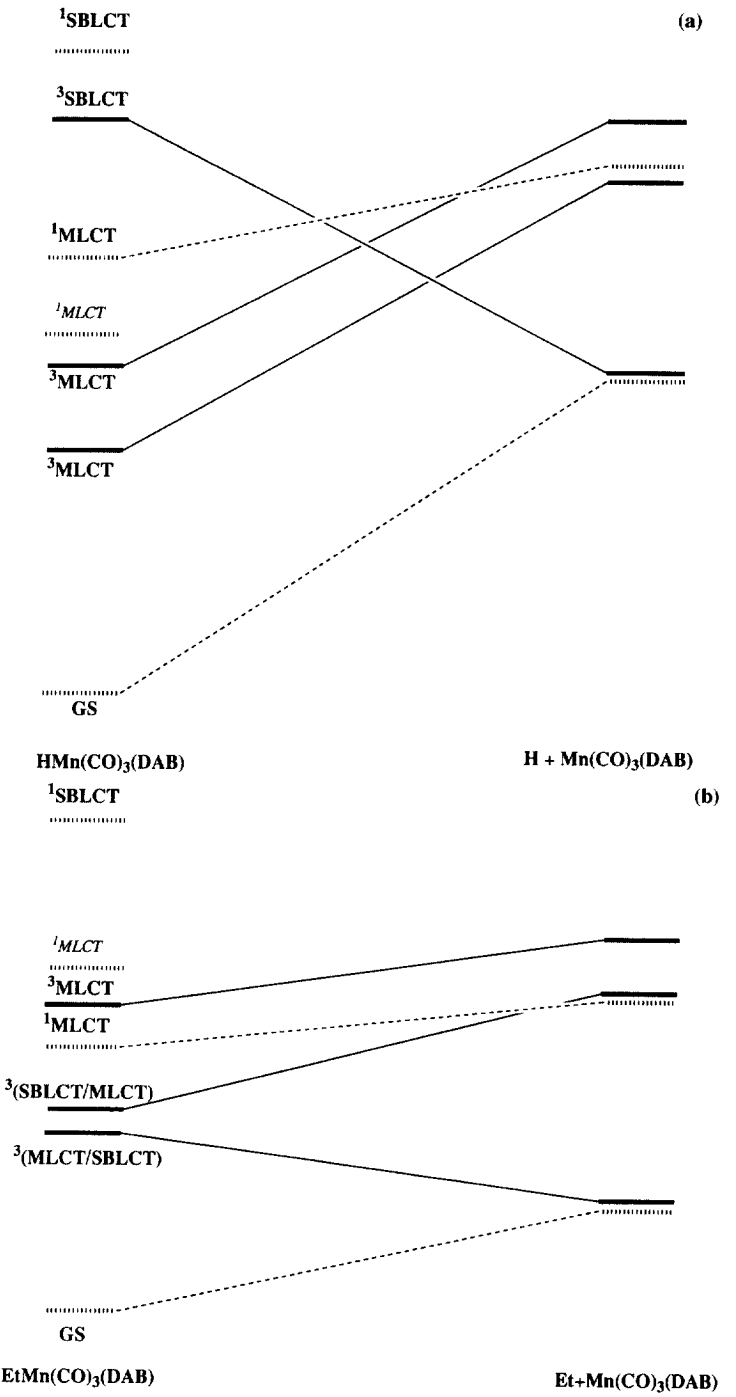

Fig. 7. State correlation diagrams connecting the low-lying electronic states of (a) Mn(H)(CO)$_3$(DAB) and (b) Mn(Et)(CO)$_3$(DAB).

distances generated by late avoided crossing with the lowest pure ^{1}MLCT state. An efficient direct homolysis along the singlet potential initially populated under visible irradiation could be possible, in contrast with the situation observed in the manganese system where high energy barriers prevent this primary reaction. The role of the triplet states should operate on a longer time scale and the long life time excited state assigned to the so called '$\sigma\pi^*$' state could be attributed to the presence of the two nearly degenerate ^{3}(SBLCT/MLCT) and ^{3}MLCT states calculated at 12600 and 13710 cm^{-1}, respectively. Further calculations are necessary to estimate the spin–orbit splitting of these low-lying triplet states and a detailed analysis of the PES calculated for the rhenium complex is needed to corroborate our hypothesis.

6. Summary

An attempt to rationalize the photochemical behavior of a series of M(R)(CO)$_3$(α-diimine) complexes has been proposed, based on a quantum chemical investigation of the excited states properties of M(H)(CO)$_3$(DAB) (M = Mn, Re) and Mn(R)(CO)$_3$(DAB) (R = H, methyl, ethyl). A qualitative mechanism of photodissociation supported by an analysis of the adiabatic PES calculated for the electronic ground and excited states (singlets and triplets) of Mn(H)(CO)$_3$(DAB) has been proposed:

1. under visible irradiation in the visible, the system gets trapped into the potential wells of the low-lying quasi-bound ^{1}MLCT excited states;
2. from there the system may dissociate towards the CO loss primary products, either directly from the singlet states on an ultra-fast time scale, or through intersystem crossing via the low-lying ^{3}MLCT states.

The presence of energy barriers along the Mn–H bond homolysis channel in Mn(H)(CO)$_3$(DAB) prevents this primary reaction, which will be characterized by a low quantum yield under visible irradiation.

A detailed analysis of the evolution of the excited states along both dissociation pathways (CO loss and Mn–H homolysis) indicates a dramatic change of electronic configuration of the triplet states on going from the equilibrium geometry to the Mn–H homolysis primary products, due to a large mixing between the ^{3}MLCT states and the ^{3}SBLCT state. Indeed, the nature of the lowest a^3A' state is modified from pure quasi-bound MLCT to dissociative SBLCT character. In contrast, these triplet states remain pure along the axial CO dissociation pathway, keeping either an MLCT character or an SBLCT character. The corresponding low-lying singlet excited states are well characterized in the FC region and remain nearly pure along both dissociation channels.

The simulation of the photodissociation dynamics of the c^1A' MLCT state, more likely populated under visible irradiation, by wavepacket propagation on the associated potential has enabled us to extract preliminary conclusions concerning the visible photochemistry.

After the initial $a^1A' \rightarrow c^1A'$ transition, on a short time scale (< 75 fs) the wavepacket evolves to the dissociation channel corresponding to axial CO elimina-

tion. The system has insufficient energy to induce the breaking of the Mn–H bond. The only alternative of deactivation on a longer time scale will be either the CO loss or the emission to the electronic ground state from the low-lying triplet MLCT states.

A comparative study of the low-lying excited states in $Mn(R)(CO)_3(DAB)$ (R = H, methyl, ethyl) and $M(H)(CO)_3(DAB)$ (M = Mn, Re) points to the following conclusions as to how ligand R and the metal center influence the photoreactivity.

On going from the hydride to the ethyl complex, the ordering and the nature of the low-lying singlet states remain similar and well defined. Therefore, the shape of the absorption spectrum should not be drastically modified inside the molecular series. However, a lowering of the ^{1}MLCT and ^{1}SBLCT states in the ethyl complex will shift the absorption spectrum to the red. In contrast, the mixed ^{3}(SBLCT/MLCT) composition of the two lowest triplet excited states in $Mn(Et)(CO)_3(DAB)$ may largely influence the photochemical behavior of this molecule. The state correlation diagrams connecting the electronic ground and excited states of $Mn(R)(CO)_3(DAB)$ (R = H, ethyl) to those of the R + $Mn(CO)_3(DAB)$ primary products indicate an efficient Mn–R homolysis primary reaction in the ethyl complex. The influence of the metal center is illustrated by the comparative study of the excited states on going from $Mn(H)(CO)_3(DAB)$ to $Re(H)(CO)_3(DAB)$: (i) a lowering of the excitation energies due to relativistic effects; (ii) a strong mixing between the ^{1,3}MLCT and ^{1,3}SBLCT excited states.

A more complete investigation of the photodissociation dynamics of $Mn(H)(CO)_3(DAB)$ should enable us to extract more quantitative information (probabilities of dissociation, branching ratio, ISC time scale) concerning the elementary processes participating in the mechanism in its early stage (below 500 fs). On a longer time scale, other factors, like geometrical distortions in the low-lying excited states or solvent effects, may largely influence the photochemical behavior of this class of molecules. The numerical simulation of these effects is beyond the scope of the present study.

A detailed analysis of the excited states and associated PESs of $Mn(Et)(CO)_3(DAB)$ has been undertaken. The main differences between the PESs of the hydride and the ethyl analog are: (i) the vanishing of the potential energy barriers along the Mn–R bond homolysis in $Mn(Et)(CO)_3(DAB)$, as expected from the state correlation diagrams, and (ii) a weaker bound character of the ^{1}MLCT states with respect to the Mn–R elongation in the ethyl complex. The consequences of these two important features will be a more efficient Mn–R bond homolysis process in an ultra-fast time scale (< 200 fs) directly from the singlet states with an opening to two concurrent dissociative channels (CO loss and Mn–R bond homolysis) and a broader absorption spectrum in $Mn(Et)(CO)_3(DAB)$.

Acknowledgements

The authors are grateful to Professor D.J. Stufkens (Amsterdam) and to the group of Professor J. Manz (Berlin) for stimulating discussions and to Dr M.C. Heitz who initiated the dynamics in Strasbourg. The authors would also like to

thank J.L. Heully, M. Pélissier and M. Dolg for their collaboration in the handling of the Effective Core Potentials. Generous financial support by the PROCOPE French/German projects 93207 is gratefully acknowledged. The quantum ab initio calculations have been carried out on the Cray-2 computer of the C98 computer of the IDRIS (Orsay, France) through a grant of computer time from the Conseil Scientifique. The quantum dynamics were performed on the workstations at the Laboratoire de Chimie Quantique, CNRS (Strasbourg).

References

[1] D.J. Stufkens, Comments Inorg. Chem. 13 (1992) 359.
[2] D.J. Stufkens, Coord. Chem. Rev. 104 (1990) 39.
[3] B.D. Rossenaar, T. van der Graaf, R. van Eldick, C.H. Langford, D.J. Stufkens, A. Vlček Jr., Inorg. Chem. 33 (1994) 2865.
[4] B.D. Rossenaar, C.J. Kleverlaan, D.J. Stufkens, A. Oskam, J. Chem. Soc. Chem. Commun. (1994) 63.
[5] J.W.M. van Outerstep, D.J. Stufkens, A. Vlček Jr., Inorg. Chem. 34 (1995) 5183.
[6] B.D. Rossenaar, M.W. George, F.P.A. Johnson, D.J. Stufkens, J.J. Turner, A. Vlček Jr., J. Am. Chem. Soc. 117 (1995) 11582.
[7] B.D. Rossenaar, C.J. Kleverlaan, M.C.E. van de Ven, D.J. Stufkens, A. Vlček Jr., Chem. Eur. J. 2 (1996) 228.
[8] B.D. Rossenaar, D.J. Stufkens, A. Oskam, J. Fraanje, K. Goubitz, Inorg. Chim. Acta 247 (1996) 215.
[9] B.D. Rossenaar, E. Lindsay, D.J. Stufkens, A. Vlček Jr., Inorg. Chim. Acta 250 (1996) 5.
[10] C.J. Kleverlaan, D.J. Stufkens, personal communication.
[11] G.J. Stor, S.L. Morrisson, D.J. Stufkens, A. Oskam, Organometallics 13 (1994) 2641.
[12] G.J. Stor, D.J. Stufkens, P. Vernooijs, E.J. Baerends, J. Fraanje, K. Goubitz, Inorg. Chem. 34 (1995) 1588.
[13] H.A. Nieuwenhuis, M.C.E. van de Ven, D.J. Stufkens, A. Oskam, K. Goubitz, Organometallics 117 (1995) 12322.
[14] H.A. Nieuwenhuis, D.J. Stufkens, A. Oskam, Inorg. Chem. 33 (1994) 3212.
[15] B.D. Rossenaar, D.J. Stufkens, A. Vlček Jr., Inorg. Chem. 35 (1996) 2902.
[16] A. Rosa, G. Ricciardi, E.J. Baerends, D.J. Stufkens, J. Phys. Chem. 100 (1996) 15346.
[17] M. Wilms, E.J. Baerends, A. Rosa, D.J. Stufkens, Inorg. Chem. 36 (1997) 1541.
[18] M.P. Aarnts, M.P. Wilms, D.J. Stufkens, E.J. Baerends, A. Vlček Jr., Organometallics 16 (1997) 2055.
[19] D. Guillaumont, K. Finger, M.R. Hachey, C. Daniel, Coord. Chem. Rev. 171 (1998) 439.
[20] K. Finger, C. Daniel, J. Chem. Soc. Chem. Commun. (1995) 1427.
[21] K. Finger, C. Daniel, J. Am. Chem. Soc. 117 (1995) 12322.
[22] M.P. Wilms, D. Guillaumont, C. Daniel, D.J. Stufkens (in preparation).
[23] A.J.H. Wachters, J. Chem. Phys. 52 (1970) 1033.
[24] I. Hyla-Kryspin, J. Demuynck, A. Strich, M. Bénard, J. Chem. Phys. 75 (1981) 3954.
[25] S. Huzinaga, Approximate Atomic Functions, Technical Report, University of Alberta, Canada, 1971.
[26] S. Huzinaga, J. Chem. Phys. 42 (1965) 1293.
[27] D. Andrae, U. Haeussermann, M. Dolg, H. Stoll, H. Preuss, Theor. Chim. Acta 77 (1990) 123.
[28] A. Bergner, M. Dolg, W. Kuechle, H. Stoll, H. Preuss, Mol. Phys. 80 (1993) 1431.
[29] P.E.M. Siegbahn, J. Almlöf, A. Heiberg, B.O. Roos, J. Chem. Phys. 74 (1981) 2384.
[30] P.E.M. Siegbahn, Int. J. Quant. Chem. 23 (1993) 1869.
[31] R. Ernenwein, M.M. Rohmer, M. Bénard, Comput. Phys. Commun. 58 (1990) 305.
[32] M.M. Rohmer, J. Demuynck, M. Bénard, R. Wiest, C. Bachmann, C. Henriet, R. Ernenwein, Comput. Phys. Commun. 60 (1990) 127.

[33] R. Wiest, J. Demuynck, M. Bénard, M.M. Rohmer, R. Ernenwein, Comput. Phys. Commun. 62 (1991) 107.
[34] M.C. Heitz, C. Daniel, Chem. Phys. Lett. 246 (1995) 488.
[35] D. Guillaumont, C. Daniel, A. Vlcek Jr., Inorg. Chem. 36 (1997) 1684.
[36] M.R. Hachey, C. Daniel, Inorg. Chem. (in press).
[37] B.D. Rossenaar, Ph.D. Thesis, University of Amsterdam, Netherlands, 1995.
[38] D. Guillaumont, C. Daniel (in preparation).
[39] R. Meyer, J. Chem. Phys. 52 (1969) 2053.
[40] C.C. Morston, C.G. Balint-Kurti, J. Chem. Phys. 91 (1989) 3571.
[41] D. Kosloff, R. Kosloff, J. Comput. Phys. 52 (1983) 35.